Response of the parameters of excess infiltration and excess storage model to land use cover change

Yuexiu Wen[1], Caihong Hu[1], Guodong Zhang[2], Shengqi Jian[1*]

[1] College of Water Conservancy & Environment, Zhengzhou University, Science road 100, Zhengzhou, China.
[2] Henan Yellow River Hydrological Survey and Design Institute, Chengdong road 100, Zhengzhou, China.
[*] Corresponding author. Tel.: +86 18603814081. E-mail: jiansq@zzu.edu.cn

Abstract: The Loess Plateau is the main source of water in Yellow River, China. After 1980s, the Yellow river water presented a significant reduction, what caused the decrease of the Yellow river discharge had been debated in academic circles. We proceeded with runoff generation mechanisms to explain this phenomenon. We built saturation excess runoff and infiltration excess runoff generation mechanisms for rainfall–runoff simulation in Jingle sub-basin of Fen River basin on the Loess Plateau, to reveal the influence of land use change on flood processes and studied the changes of model parameters under different underlying conditions. The results showed that the runoff generation mechanism was mainly infiltration-excess overland flow, but the flood events of saturation-excess overland flow had an increasing trend because of land use cover change (the increase of forestland and grassland areas and the reduction of cultivated land). Some of the model parameters had physical significances，such as water storage capacity (WM), infiltration capacity (f), evapotranspiration (CKE), soil permeability coefficient (k) and index of storage capacity distribution curve (n) showed increasing trends, and index of infiltration capacity distribution curve (m) showed a decreasing trend. The above results proved the changes of runoff generation mechanism from the perspective of model parameters in Jingle sub-basin, which can provide a new perspective for understanding the discharge reduction in the Yellow River basin.

Keywords: Land use; Saturation excess and infiltration excess model; Model parameters; Fen River.

INTRODUCTION

Intensive soil erosion, soil desertification, and vegetation degradation are features of the soil and water transition zone in the Loess Plateau region in China (Gao et al., 2018). Numerous vegetation restoration measures have been implemented by the Chinese government, including the planting of perennial shrubs and grasses, in an attempt to restore the environment and reduce soil and water loss in the region. Improving the hydrological aspects of the environment via ecological restoration is two-tiered and involves (1) the prevention of water and soil loss by altering water cycle paths. Indigenous perennial plants can achieve this by increasing the effective vegetation coverage and thus minimizing surface runoff. The second aspect is related to (2) increasing the soil moisture content in order to effectively enhance productivity (Desilets et al., 2007).

Climate change may be a significant driver of changes in the flood frequency which has been widely investigated (Viglione et al., 2016). And many studies have reported that land cover change had an effect on the water cycle and resulted in variations in water resources supply and demand (Finch et al., 2004; Molina et al., 2012). However, there are only a few studies on the role of land use change in modifying river floods. Land use change has, potentially, a very strong effect on floods as humans have heavily modified natural landscapes. Large areas have been deforested or drained, thus either increasing or decreasing antecedent soil moisture and triggering erosion (Rogger et al., 2017). The Loess Plateau is the main source of water in Yellow River, China. After 1980s, the Yellow river discharge presented a significant reduction, what caused the decrease of the Yellow river discharge had been debated in academic circles. Liu et al. (2018) reported that vegetation restoration in Loess Plateau would result in water reduction in

the Yellow River, however, Mu et al. (2013) found that climate change played a decreasing role in runoff reduction comparing with vegetation restoration. Also, Rozalis et al. (2010) pointed out that it was necessary to study the hydrological impacts of land use changes because that it was still controversial. But most studies focused on quantitative analyses of the effect of land use on water circle. There is a great need to study the effect of this change on future environmental flows.

Hydrological model is a generalization of hydrological phenomena in nature and often used to simulate hydrological processes (Park and Markus, 2014). From the scientific and complex degree of reflecting the rules of physical motion of water flow, there are mainly three types of models (Meng et al., 2017): conceptual models, systematic models (black box models) and physical-based models (Calver, 1988; Lee et al., 2005; Kan et al., 2017). Through accurate modeling of rainfall-runoff dynamics, it not only provides flood warnings to reduce disasters, but also enhances proper reservoir management during drought periods. However, the process of rainfall runoff conformation is affected and restricted by many factors (such as temporal, spatial variability of basin characteristics, rainfall, and coverage of vegetation). According to Grayson et al. (1992), conceptual models are better than physically based models since they are faster computationally and have less number of parameters when the suitable scale is adopted. Sorooshian et al. (1993) indicated that conceptual rainfall-runoff models are difficult to calibrate using automatic methodologies. The successful application of a conceptual rainfall-runoff model depends on how well the model is calibrated. Beven (1989) had presented the limitations of current rainfall-runoff models and argued that the possible way forward must be based on a realistic assessment of predictive uncertainty. With the increasing enrichment of distributed hydro meteorological information

and underlying surface information (such as rainfall, temperature, land use and soil properties) and the rapid improvement of computer, the development of physical-based distributed hydrological models have been a research hot spot (Apostolopoulos et al., 1997; Blyth, 1993).

Flood simulation and prediction is one of the most active researching areas in surface water hydrology. Flood takes place whenever there is a heavy or a long period of precipitation. An accurate prediction of flood under changeable meteorological and layer conditions can not only help in the water resources management especially in hydropower, but also reduce the loss of lives and property to the minimum in floodplain areas. A special problem in hydrological model simulation analysis is model parameters. The general idea of parameters in dynamic models is that they represent the stable catchment conditions while the rainfall and other inputs are the time-varying boundary conditions. In most cases, some level of model calibration will be useful to reduce bias (Beven, 2000a,b). Du et al. (2016) used Xinanjiang model to simulate runoff of the reservoirs and flood hydrology graphs of all sub-catchments of the basin, and simple reservoir operation rules were established for calculating effluent of the reservoirs. But, the runoff model of basin is not single, with the change of rainfall conditions, including both saturation excess runoff and infiltration excess runoff. At this time, it is often difficult to obtain satisfactory results if only one runoff model is adopted for calculation (Luo et al., 1992). However, under the influence of climate change and human activities, the consistency hypothesis in the traditional hydrological simulation process has been questioned (Ren et al., 2016), and the assumption that the basin hydrological model parameters are constant over time is no longer applicable. On the one hand, the structural and data problems of the model and on the other hand, the changes of the boundary conditions of the basin, such as changes in the land use may result in changes in the model parameters (Andreássian et al., 2003; Brown et al., 2005; Wagener et al., 2003). There are similar parameters in continuous runoff models related to runoff generation that may

also vary in response to climate fluctuations. However, just how calibrated model parameters change with time is currently not very well understood (Wagener et al., 2010). In order to account for any changes in the parameters caused by changes in the catchment characteristics, a unique relationship between the two would be needed, but often, there are complex correlations among the parameters and with various catchment characteristics (Wagener, 2007). Therefore, it is necessary to study the variation of hydrological model parameters in a changing environment to improve the simulation accuracy and study the rules of model parameters.

The objective of this study is to (1) to build a new conceptual model for simulating effect of land use change on floods, to reveal the influence of land use change on flood processes; (2) study the changes of model parameters under different underlying conditions.

METHODOLOGIES
M-EIES model

The M-EIES model was improved on the basis of the Xinanjiang model. The original Xinanjiang model just considers excess storage runoff, which is based on the water storage capacity distribution curve of the basin, with poor practicality in semi-arid and semi-humid areas (Zhao, 1992). In the M-EIES model, the excess infiltration runoff part is added on the basis of excess storage, which is based on the basin infiltration curve and the infiltration capacity distribution curve of the basin. Compared with the Xinanjiang model, in M-EIES model, the excess infiltration runoff mode is based on the basin infiltration curve and the infiltration capacity distribution curve of the basin, and the storage runoff mode is based on the water storage capacity distribution curve of the basin. According to the characteristics of runoff in the Loess Plateau, the two types of runoff modes are organically combined. Moreover, according to the characteristics of different land use types, different infiltration and evaporation are adopted in the M-EIES model.
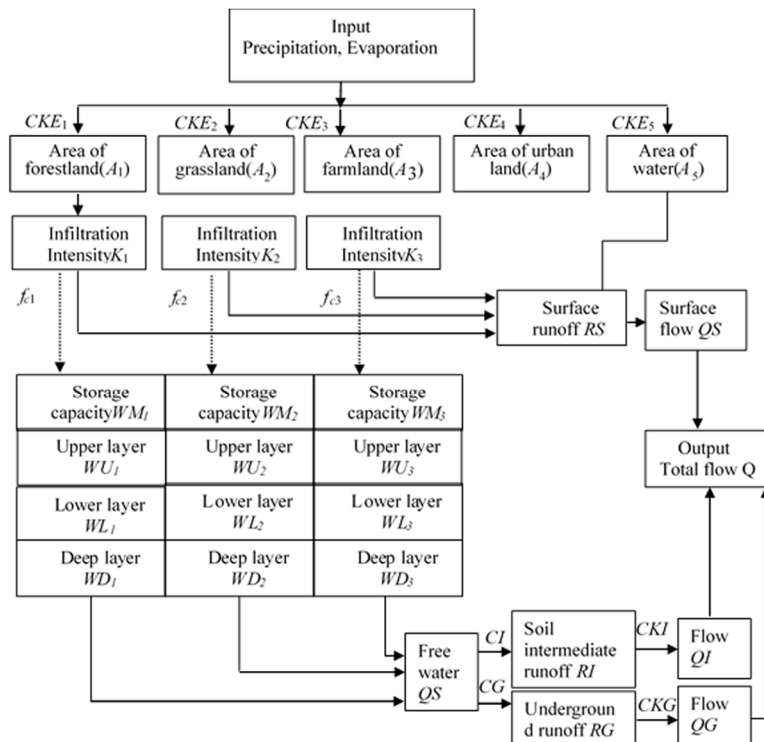

Fig. 1. Structure of *M-EIES* model.

According to the use of the free water storage capacity curve to divide the water source into surface runoff (*RS*), soil intermediate runoff (*RI*) and underground runoff (*RG*), the complex runoff formation process is transformed into the relationship between the water storage capacity and the runoff of the basin. It satisfies the different conditions that the movement process of different water sources in the outlet section of the basin is affected by the regulation and storage of the basin. A schematic diagram for *M-EIES* model is shown in Fig. 1.

Under the condition of sufficient water supply, the average infiltration rate curve of each point in the basin is called the infiltration capacity curve of the basin, which is also called the infiltration capacity curve of the basin. Many data indicate that the Horton infiltration formula and the measured points are well fitted and have a certain theoretical basis as follow:

$$f = f_c + (f_0 - f_c)e^{-kt} \tag{1}$$

where *f* is the infiltration capacity at time *t*; f_c is the steady infiltration rate (mm/h); f_0 is the initial infiltration capacity (mm/h); and *k* is the index related to soil permeability characteristics (h^{-1}). In this study, different infiltration rates were used to simulate forestland, grassland and cultivated land.

The infiltration capacity of the basin during the period is expressed as the mean value of the infiltration water volume in the basin during the period when the water supply is sufficient. For the integral of the infiltration capacity curve of the basin in the time period, the calculation formula is as follows:

$$F_{m\Delta t} = \int_t^{t+\Delta t} f dt = f_c \Delta t + \frac{1}{k}(f_0 - f_c)e^{-kt}(1 - e^{-k\Delta t}) \tag{2}$$

where, $F_{m\Delta t}$ is infiltration capacity during the basin; others are the same as Eq. (1).

According to experience (Luo et al., 1992), the parabolic equation of m times is used to represent the distribution curve on the watershed, and the formula is:

$$\beta = 1 - (1 - \frac{F'_{\Delta t}}{F'_{m\Delta t}})m \tag{3}$$

$$F_{m\Delta t} = \int_0^t F'_{\Delta t} d\beta = \int_0^{F'_{m\Delta t}} (1 - \beta)dF'_{\Delta t} = \frac{F'_{m\Delta t}}{m+1} \tag{4}$$

$$F'_{m\Delta t} = (m+1)F_{m\Delta t} \tag{5}$$

where, $F'_{\Delta t}$ is the infiltration capacity of certain point; $F'_{m\Delta t}$ is the maximum infiltration time of the basin; *m* is an empirical index; *β* is the relative area.

Where *SM* is the free water storage capacity of the basin; *S* is the average water storage depth on the flow area, *R* is runoff. If *R+S > SM*, then:

$$RS = R + S - SM \tag{6}$$

$$RI = CI \times SM \tag{7}$$

$$RG = CG \times SM \tag{8}$$

when *R+S ≤ SM*, then: $RS = 0 \tag{9}$

$$RI = CI \times (R + S) \tag{10}$$

$$RG = CG \times (R + S) \tag{11}$$

where *RS* is surface runoff; *RI* is soil intermediate runoff; *RG* is underground runoff; *CI* is outflow coefficient of soil; *CG* is underground runoff coefficient.

The model considers the water storage capacity at each point of the basin differently. According to experience, the parabolic type is introduced into the water storage capacity distribution curve.

$$\partial = 1 - (1 - \frac{W'}{W'_m})^n \tag{12}$$

where *W'* is the storage capacity value of a certain point; W'_m is the maximum water storage capacity of the basin; *n* is the empirical index; *∂* is the relative area, indicating the ratio of the area under *W'* to the total drainage area.

$$W_m = \int_0^{W'_m}(1 - \partial)dW' = \frac{W'_m}{n+1} \tag{13}$$

where W_m is average water storage capacity of the basin.

The surface runoff calculation uses the instantaneous unit line method to simulate the ground confluence process of the basin. The confluence calculation of the soil middle stream and the underground runoff is calculated by the linear reservoir storage model.

Compared with the original model (16 model parameters), the *M-EIES* model have 24 parameters, some of them have physical significances, including *WM*, f_c, *C*, *m*, *n*, *k* and *CKE*, which would be obtained by the basin feature statistics. Others are the process parameters, which would be obtained by the parameter optimization. The model parameters can be grouped into four categories based on the model module, (1) evapotranspiration parameters, including *WUM*, *WLM*, *C*, CKE_1, CKE_2, CKE_3 and CKE_4; (2) flow parameters, including *WM*, *m*, *n*, f_{c1}, f_{c2}, f_{c3}, k_1, k_2 and k_3; (3) water source parameters, including *SM*, *EX*, *CI* and *CG*; (4) confluence parameters, including *CKI*, *CKG*, *N* and *NK*. The concepts of these parameters are presented in Table 1.

Model calibration and validation parameter optimization

To analyze the impact of land use change on flood process, we established *M-EIES* model based on land use. Combined with the land use data, we divided the flood event into three stages and calibrated and validation each stage. The calibration makes use of an objective functionthat involves theNash-Sutcliffe efficiency coefficient (*NSE*) and the coefficient of determination (R^2) and the relative error (R_e).

The *NSE* was proposed by Nash and Sutcliffe (1970) is as follow:

$$NSE = (1 - \frac{\sum(Q_i - Q_{si})^2}{\sum(Q_i - Q_m)^2}) \tag{14}$$

where Q_i, the measured discharge (m^3/s); Q_{si}, the simulated discharge (m^3/s); Q_m, the averaged measured discharge (m^3/s).

The coefficient of determination (R^2) is expressed as

$$R^2 = (\frac{\sum(Q_{si} - Q_{sm})(Q_i - Q_m)}{\sqrt{(Q_{si} - Q_{sm})^2}\sqrt{(Q_i - Q_m)^2}})^2 \tag{15}$$

where Q_{sm} the averaged simulated discharge (m³/s). Other symbols have the same meanings.

The relative error (R_e) is used to evaluate the difference between observed discharge and model simulated discharge.

$$R_e = \left| \frac{\sum(Q_i - Q_{sm})}{\sum Q_i} \right| \times 100\% \quad (16)$$

In calibration procedures, the parameter values are usually bounded between two limits (Duan et al., 1992). The bounds are given (Table 1). However, some parameters are not the result of a single process or a single influencing factor, so it is unlikely to be determined by actual measurement. It can only rely on the system method and solve with the optimization technique. In this study, we mainly use *SCE-UA*. The *SCE-UA* combines the strengths of the simplex procedure with: (1) the concept of controlled random search; (2) competitive evolution; (3) the concept of complex shuffling. The synthesis of these three concepts makes the *SCE-UA* robust, flexible and efficient (Duan et al., 1992). First, according to the physical meaning of the model parameters, we gave the initial value of the model parameter (Table 6), and then the *SCE-UA* was further preferred to obtain the approximate optimal values of the various parameters of the model.

STUDY AREA AND DATA
Study area

The Fen River, being located in the Shanxi province in northern China, is one of the largest tributaries of the Yellow River. The drainage area of the Fen River basin is 39471 km². The river basin has a temperature continental monsoon climate with monthly average air temperature varies from 4 to 13°C and the maximum evaporation capacity of the water surface is 1120mm. The area has an average annual precipitation of 503 mm, 60% of which occurs between July and September. The average annual runoff of the basin was 57.9mm. The major land use type of this area is forest and farmland, although the construction land of towns has extended year by year with the fast pace of urbanization since the 1980s, in Jingle sub-basin. Which located in the north and upper reaches of Fen River basin, was selected as case studies (Fig. 2).

The drainage area of sub-basin (Jingle) is 2799 km² with a large number of floods. The main channel length is 83.9 km, the average slope of the main stream is 6.7%, the shape coefficient of the basin is 0.398. The underlying surface conditions changed greatly since 1980s, the "Grain for Green" project was conducted, which has a great impact on water resource and flood (Uchida et al., 2005). In addition, there is no coal mining activity, the amount of water diversion is small and no water conservancy projects in the Jingle sub-basin.

Table 1. The meanings of the *M-EIES* model parameters.

| Parameter	Parameter meaning	Range	Parameter	Parameter meaning	Range
WM	Average catchment storage capacity	100–200	fc_3	Farmland steady infiltration rate	4–6
n	Index of storage capacity distribution curve	0.01–0.7	k_3	Farmland soil permeability coefficient	0.1–0.8
m	Index of infiltration capacity distribution curve	0.01–0.7	CKE_4	water area evaporation conversion	0.5–2
C	Deep evaporation coefficient	0.01–0.4	SM	Free water storage capacity	10–20
CKE_1	Forest land evaporation conversion	0.5–2	EX	Index of free water storage capacity curve	1–5
fc_1	Forest land steady infiltration rate	4–6	CI	Outflow coefficient of soil	0.01–0.7
k_1	Forest land soil permeability coefficient	0.1–0.8	CG	Underground runoff coefficient	0.01–0.7
CKE_2	Grass land evaporation conversion	0.5–2	CKI	Extinction coefficient of flow in soil	0.9–1
fc_2	Grass land steady infiltration rate	4–6	CKG	Extinction coefficient of underground runoff	0.9–1
k_2	Grass land soil permeability coefficient	0.1–0.8	N	River convergence parameter	\
CKE_3	Farmland evaporation conversion	0.5–2	NK	River convergence parameter	\
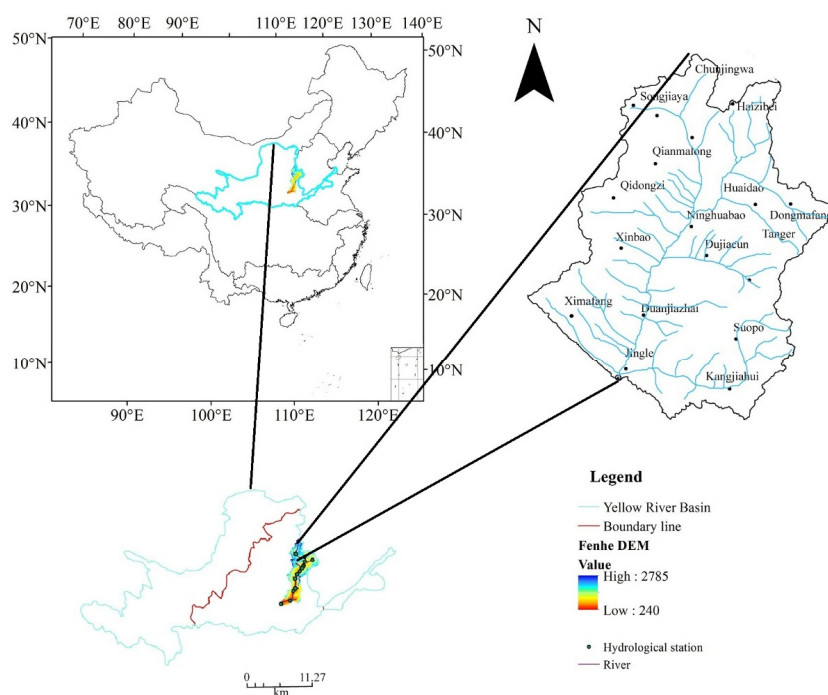
Fig. 2. Locations of the Fen River basin and Jingle sub-basin.

Dataset

We got the Landsat Thematic Mapper (TM) imagery of the years 1978, 1998 and 2010 from Global Land Cover Facility which were used to show the variation of land use in the experimental period (Fig. 3). The digital elevation model (DEM) with a spatial resolution of 30 m was downloaded from China Soil Scientific Database (CSSD). Soil type data of the sub-basin was gotten from Consultative Group on International Agricultural Research-Consortium for Spatial Information (CGIAR-CSI). The hydrological data included precipitation, evaporation and runoff from 1965 to 2014. There are 16 hydrological stations in the Jingle sub-basin of the Fen River basin, about 1 per 175 km^2. Area-averaged rainfall and evaporation are obtained from Thiessen polygon method. The basin-averaged minimum required hourly input data for basin are: rainfall and evaporation. And hydrological stations were extracted from <<Data of the Yellow River basin>> (http://www.yrcc.gov.cn/). During the study period (from 1965 to 2014), 63 flood events were observed, we selected 29 flood events to build the *M-EIES* model.

Table 2 and Table 3 showed the detailed information of the land use change. From 1978 to 1998, the areas of farmland and grassland changed greatly. The farmland decreased by 74.14 km^2, the grassland decreased by 22.02 km^2, and the woodland area increased by 96.7 km^2, which was mainly caused by the conversion from grassland and cultivated land to woodland. From 1998 to 2010, the areas occupied by farmland, grassland and forest changed greatly. Among them, the farmland decreased by 109.11 km^2, the grassland increased by 42.8 km^2, and the woodland increased by 65.9 km^2, showing the conversion from farmland to grassland, from grassland and farmland to woodland. Water areas and urban construction land have changed not much.

Table 2. Land use transfer matrix from 1978 and 1998.

1998 / 1978	Farmland/km^2	Forest/km^2	Grass/km^2	Water/km^2	Urban/km^2	Total/km^2
Farmland/km^2	679.41	13.52	64.95	0.02	0.22	758.12
Forest/km^2	0.64	894.24	4.65	0.00	0.00	899.53
Grass/km^2	3.90	88.30	996.14	0.12	0.09	1088.55
Water/km^2	0.00	0.00	0.45	35.76	0.00	36.21
Urban/km^2	0.03	0.16	0.34	0.00	16.05	16.58
Total/km^2	683.98	996.23	1066.53	35.90	16.35	2799.00

Table 3. Land use transfer matrix from 1998 and 2010.

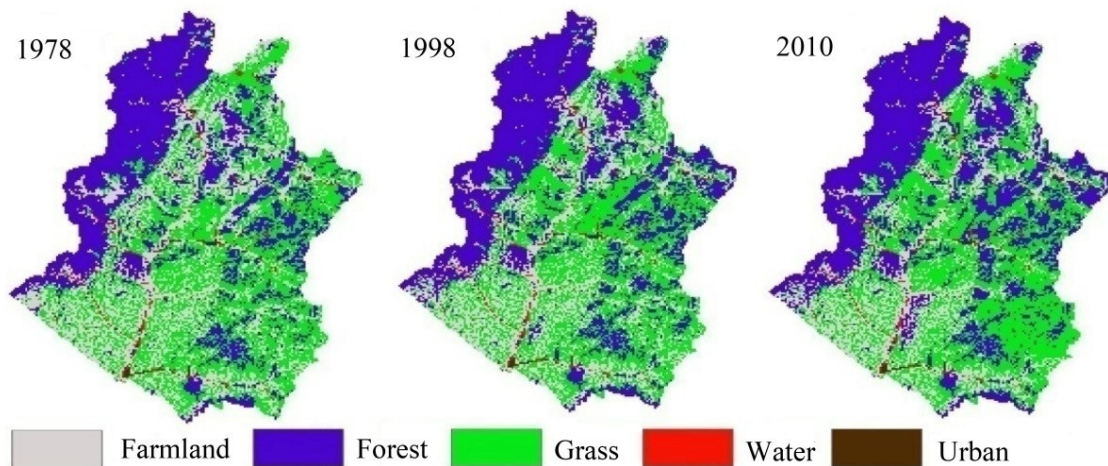| 2010 / 1998	Farmland/km^2	Forest/km^2	Grass/km^2	Water/km^2	Urban/km^2	Total/km^2
Farmland/km^2	568.99	13.55	100.95	0.23	0.04	683.77
Forest/km^2	0.91	987.02	8.38	0.00	0.14	996.45
Grass/km^2	4.71	61.57	999.69	0.37	0.18	1066.52
Water/km^2	0.05	0.10	0.12	35.64	0.00	35.91
Urban/km^2	0.00	0.11	0.25	0.00	16.01	16.36
Total/km^2	574.66	1062.35	1109.38	36.24	16.37	2799.00

Fig. 3. Land uses of the Jingle sub-basin.

RESULT AND DISCUSSION
Runoff characteristics

The time periods from 1965 to 2014 were divided into three periods (1965–1978, 1979–1998 and 1999–2014) (12 flood events from 1965 to 1978, 12 flood events from 1979 to 1998, and 6 flood events from 1999 to 2014). Due to the influence of rainfall and underlying surface changes, runoff coefficient has an obvious decreasing trend from 1965 to 2014 (Fig. 4), which indicated that with the change of land use, the runoff yield and confluence conditions of the basin changed greatly, resulting in the change of flood process of the basin outlet section. The rainfall-runoff relationship at each stage is different. The rainfall-runoff correlation coefficients of each stage were 0.80, 0.64

and 0.57, respectively. In comparison, the third-stage runoff has the strongest dependence on rainfall, and the runoff in the third stage has decreased significantly (Fig. 5A). The R^2 were 0.58, 0.55 and 0.51 between rainfall intensity and runoff in each stage, respectively. For the rainfall events of the same magnitude of rainfall intensity, in the three stages, the first stage has the largest runoff and the third stage has the smallest runoff (Fig. 5B), which indicated that the effect of underlying surface conditions change on runoff was increasingly intensified.

Flood simulation

During the period of 1965–1978, we selected 12 flood events (8 flood events for model calibration and 4 flood events for model validation) with the flood peaks from 216 to 2165 m^3/s. 11 and 6 flood events were selected from 1979 to 1998 (7 flood events for model calibration and 4 flood events for

model validation), from 1999 to 2014 (4 flood events for model calibration and 2 flood events for model validation). The Xinanjiang model and the *M-EIES* model were used to calculate the runoff (Table 4).

From 1965 to 1978, Nash–Sutcliffe efficiency coefficient (*NSE*) of all floods were greater than 0.7; the coefficient of determination (R^2) were greater than 0.8, and the relatively error (R_e) was smaller than 6% at the hourly scale. From 1979 to 1998 and 1999 to 2014, The *NSE* of floods were greater than 0.7; the R^2 were greater than 0.8, and the R_e were smaller than 15%. The simulated and observed values for Jingle sub-basin was shown in Fig. 6, Fig. 7, Fig. 8 and Fig. 9. These three indices (*NSE*, R^2 and *Re*) of the Xinanjiang model were compared with that of the *M-EIES* model (Table 5). The *NSE* of *M-EIES* model was greater than 0.7 for both calibration and validation period no matter what period. However, the *NSE* of Xinanjiang model was just about 0.5 in calibration and validation period.

Table 4. Simulation results of Jingle sub-basin in the calibration and validation periods in the three stages.

| Stages		Flood time	*NSE*	R^2	*Re* (%)	Number of hours(h)
1965–1978	Calibration	19660815	0.96	0.81	9.2	67
		19670810	0.90	0.79	14.4	176
		19690726	0.80	0.82	14.4	57
		19690806	0.88	0.87	1.9	178
		19710701	0.71	0.75	14.7	40
		19710807	0.74	0.81	13.4	34
		19730819	0.86	0.86	15.5	107
		19740706	0.81	0.81	13.5	54
	Validation	19750805	0.92	0.80	1.5	48
		19770706	0.91	0.75	0.4	110
		19770802	0.91	0.66	2.3	56
		19780808	0.88	0.74	12.0	75
1979–1998	Calibration	19810722	0.78	0.88	9.1	48
		19810805	0.77	0.87	11.5	72
		19830821	0.75	0.83	10.6	48
		19850511	0.79	0.84	12.4	46
		19880720	0.81	0.84	15.2	60
		19890721	0.76	0.79	11.3	87
		19920831	0.72	0.84	6.5	165
	Validation	19940706	0.87	0.81	9.4	102
		19960614	0.79	0.76	9.9	79
		19960719	0.88	0.72	11.5	95
		19980630	0.75	0.79	14.5	76
1999–2014	Calibration	20010711	0.75	0.84	13.4	36
		20010720	0.78	0.86	9.5	84
		20020811	0.85	0.87	8.7	103
		20080923	0.90	0.82	10.1	181
	Validation	20110729	0.88	0.87	9.3	117
		20130715	0.78	0.77	14.6	180
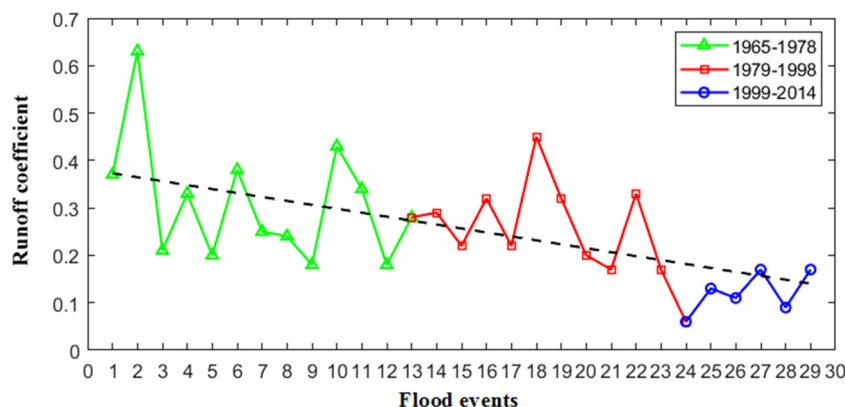
Fig. 4. Variation trend of flood runoff coefficient in the Jingle sub-basin from 1965 to 2014.
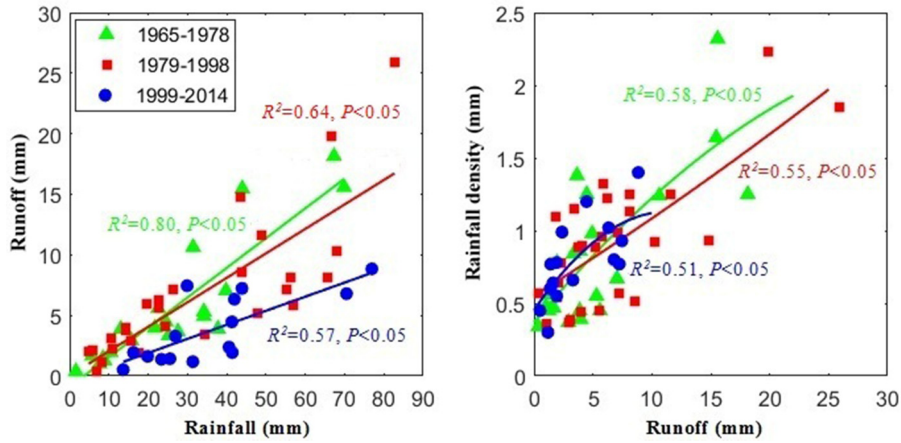
Fig. 5. The relationships between rainfall and runoff for per flood (The left is Fig. 5A, the right is Fig. 5B. The green line is the trend line from 1965 to 1978; red line: 1979–1998; blue line: 1999–2014).
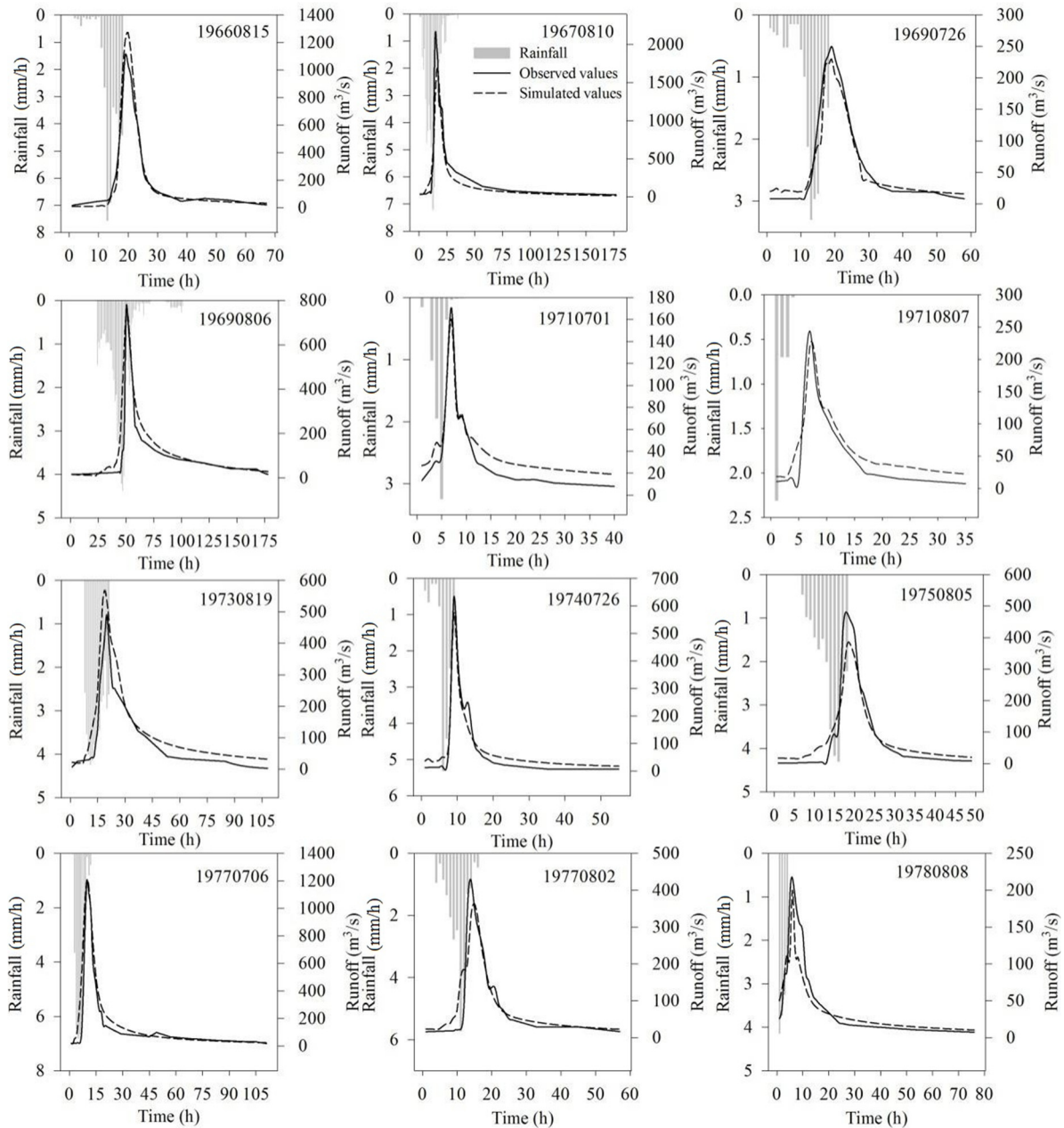

Fig. 6. Simulation results of Jingle sub-basin in the calibration and validation periods from 1965 to 1978.
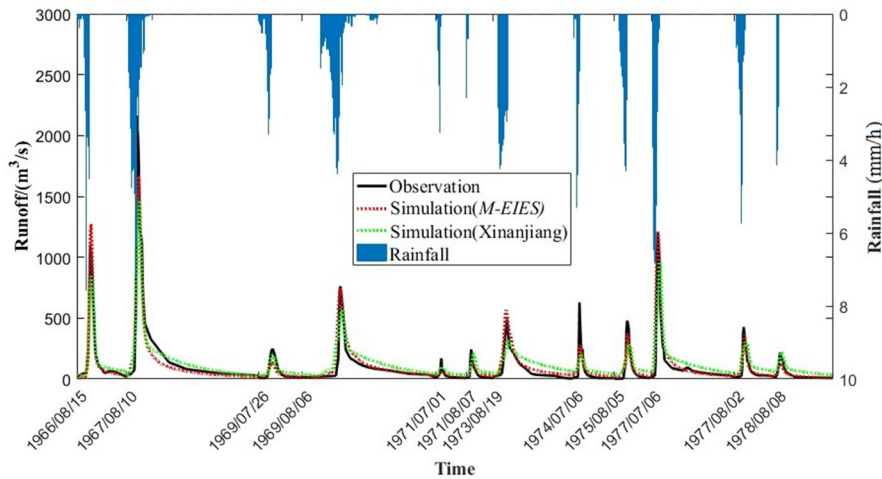
Fig. 7. Simulation results of Jingle sub-basin from 1965 to 1978 (The time step is 1 hour).
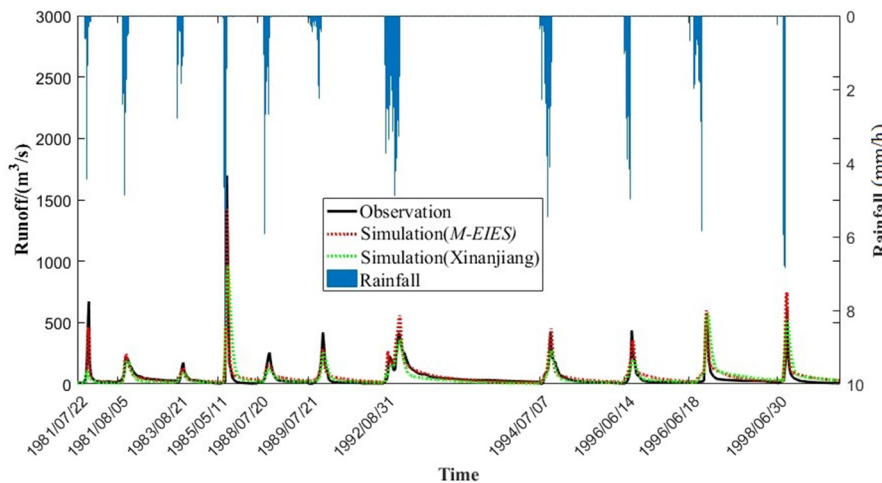

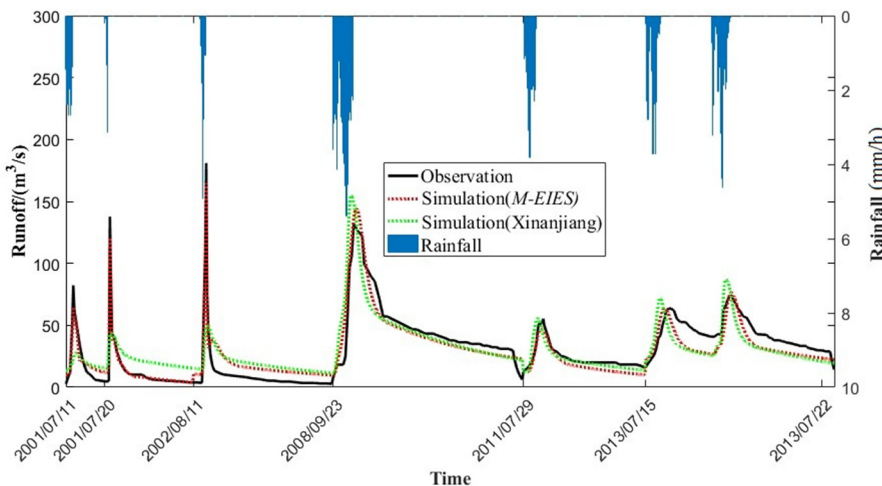**Fig. 8.** Simulation results of Jingle sub-basin from 1979 to 1998 (The time step is 1 hour).

Fig. 9. Simulation results of Jingle sub-basin from1999 to 2014 (The time step is 1 hour).

Similarly, the R^2 of *M-EIES* model varying from 0.72 to 0.85 in calibration and validation period were greater than that of Xinanjiang model. In addition, the *Re* of *M-EIES* model was obviously smaller than that of Xinanjiang model. The results indicated that *M-EIES* model performed well in Jingle sub-basin and can be used to simulate runoff with different land use stages.

The climate change and human activities have influences on model parameters. In each stage, we selected several floods events to calibrate model parameters, respectively. The simulation accuracy can be improved, due to considering the effects of land use changes on the flood process. The same method can be found in some studies (Pathiraja et al., 2016; Wallner and Haberlandt, 2015).

Table 5. The results of *NSE*, R^2, and *Re* in calibration and validation periods.

Stages		M-EIES			Xinanjiang model		
		NSE	R^2	Re (%)	NSE	R^2	Re (%)
1965–1978	Calibration	0.83	0.72	12.12	0.54	0.56	18.45
	Validation	0.91	0.74	4.05	0.57	0.64	16.54
1979–1998	Calibration	0.77	0.84	10.94	0.48	0.57	19.78
	Validation	0.83	0.77	11.32	0.52	0.62	22.54
1999–2014	Calibration	0.82	0.85	10.42	0.56	0.54	15.43
	Validation	0.83	0.82	11.95	0.58	0.62	13.25

M-EIES model parameters and land use cover changes
Parameters for physical significances

The model parameters in the three stages were presented in Table 6. It can be seen that different land use types reflect different values of runoff parameters. To analyze this, we discuss different types of parameters and study the effects of land use change on them. (Merz et al., 2008) argued that long-term interactions, climate change and changes in land characteristics can affect model parameters, but they are considered small for the 30 years considered. But in this study, land use change is booming, for most models, the parameters also vary significantly. For example, the *f* and *CKE* of different land use types are different. (Xie et al., 2007) got the same conclusion. The parameters, *WM*, *f*, *CKE* and *k* showed increasing trends during the experimental period. Vegetation is closely related to the soil water permeability, water holding capacity and water storage capacity. The soil compactness would increase with degraded vegetation, resulted in the reduction of soil saturated hydraulic conductivity, infiltration rate and water storage capacity. The surface runoff would increase with the decreased underground runoff (Wang et al., 2015). Vegetation could increase rainfall infiltration by improving the soil organic matter and soil porosity. Therefore, land use cover changes are the important reason for rainfall-runoff characteristics (Gonzalez-Sosa et al., 2010), which has an influence on the processes of runoff generation and confluence by affecting groundwater outflow capacity, infiltration capacity and watershed water storage capacity (Pirastru et al., 2013).

(1) Groundwater outflow capacity
In the Jingle sub-basin, the forest area increased rapidly. Previous studies found groundwater outflow capacity had an influence on underground water, and the minimum daily discharge and the minimum daily discharge in flood season could reflect the discharge capacity of groundwater (Table 7). The annual mean minimum daily flow and the minimum daily flow in the flood season showed the obvious trends in the three stages. In the flood season, more rainfall, the groundwater recharge increased. Under the similar rainfall conditions, groundwater outflow capacity is stronger from 1999 to 2014, which is easier to generate underground flow and interflow, resulted in the decrease of flow. The confluence time expanded and changed the process of flood. The 12.08% increase in forest areas resulted in the 45.37% increase in groundwater outflow capacity.

(2) Infiltration capacity
The forest areas increased by 12.08%, averaged rainfall depth before generate flow increased by 157.67% and the duration of flood subsidence increased by 14.51% (Table 7). In the early stage of storm, the rainfall is mainly consumed by the infiltration. Flood subsidence is an important part of runoff generation and confluence. There is a certain amount of infiltration during the process of flood subsidence. Generally speaking, with the increase of rainfall and rainfall intensity, runoff coefficient will

Table 6. The *M-EIES* model parameters in the three stages.

Model parameters	Initialization parameter	1965–1978	1979–1998	1999–2014
WM	150	101.369	124.731	156.36
X	0.2	0.15	0.143	0.283
Y	0.3	0.201	0.252	0.296
n	0.1	0.586	0.418	0.365
m	0.1	0.065	0.175	0.169
C	0.1	0.133	0.126	0.318
CKE_1	1	0.901	0.989	1.104
f_{c1}	4.5	4.986	4.991	5.231
K_1	0.5	0.381	0.231	0.348
CKE_2	1	0.531	0.893	0.985
f_{c2}	4	4.868	4.957	5.024
K_2	0.5	0.15	0.306	0.415
CKE_3	1	1.04	1.113	1.423
f_{c3}	3.8	4.02	4.458	4.89
K_3	0.5	0.385	0.426	0.441
EX	3	3.761	2.97	2.67
SM	12	12.815	14.474	16.088
CKG	0.8	0.918	0.983	0.99
CKI	0.8	0.986	0.948	0.999
CI	0.5	0.458	0.126	0.37
CG	0.3	0.139	0.121	0.203
N	3	3.189	3.189	3.505
NK	2.5	3.315	1.404	1.892

increase. As the years processed, more rainfall was needed in the Jingle sub-basin to produce runoff, indicating the infiltration increased gradually. Also, the duration of flood subsidence increased gradually (Table 7). The increase of infiltration is an important reason for changes of runoff generation and confluence mechanism in the basin. The increase of soil moisture enhancement, resulted in the decrease of surface runoff, runoff coefficient and flood peak flow, increase of underground runoff and confluence duration (Ogden et al., 2011). Also, our previous study found that the flood events of saturation excess over land flow increased with the decrease of flood events of infiltration-excess over land flow, due to the increase of forest areas (Li, 2018).

Forests and grass had greater steady infiltration rates than farmland (Table 6). Vegetation influences the chemistry, structure, organic content, and strength of soils. Roots and burrowing organisms' bioturbated soils, changing the pathways and generally increasing porosity and infiltration capacity (Moussa et al., 2002). As a consequence, alterations in vegetation may create broad-scale changes in the way rainfall is partitioned into runoff and recharge. Infiltration capacity is a commonly used term which is the maximum rate at which soils can absorb water, generally occurring under dry conditions when sportive influences are greatest. The infiltration capacity tends to decrease as the soil moisture content of the surface layers increases (Jian et al., 2014). In general, deeper rooted species can change

Table 7. Daily flow, averaged rainfall depth before generate flow and Duration of flood subsidence in the three stages.

Items	1965–1978	1979–1998	1999–2014
Forest areas (km²)	899.53	996.23	1062.35
Annual mean minimum daily flow (m³/s)	0.68	1.26	1.40
Minimum daily flow in the flood season (m³/s)	1.93	2.61	3.30
Averaged rainfall depth before generate flow(mm)	6.9	9.4	21.0
Duration of flood subsidence (h)	14.22	14.39	16.38
Catchment water storage capacity (mm)	101.37	124.73	156.36

soil properties to suit their needs of water use (Yüksek et al., 2009). There are spatial variations in hydrology and soil characteristics which are not represented in this analysis, and those differences are likely the reason for the large differences of site-to-site. For example, bare soil in one location may have higher infiltration than grasses at another location, likely attributable to other soil forming factors such as parent material, topography, aspect, climate, and soil age. However, this study does show promise for generalization of local or perhaps even island-wide trends, which would allow for mappable units of infiltration properties that can be related to processes of interest including areas of potentially high aquifer recharge or erosion susceptibility.

(3)   Water storage capacity

The water storage capacity of the Jingle sub-basin increased year by year. Previous studies have shown that the water storage capacity of woodland is higher than other land use covers, and the increase of forest areas would result in the increase of catchment water storage capacity, and reducing runoff (Jian et al., 2016). The forest areas increased by 12.08% with the water storage capacity increased by 27.84% (Table 6), other studies had found the similar results (Zhang et al., 2014). The water storage capacity distribution curve index (n) and the infiltration capacity distribution curve index (m) are the main indicators to determine the runoff generation mechanism. When $m = 0$, it is a typical flood event of saturation-excess overland flow; when $n = 0$, it is a typical flood event of infiltration-excess overland flow. In Jingle sub-basin, both saturation-excess overland flow and infiltration-excess overland flow existed (Table 5). Our previous study found that the flood events were mainly infiltration-excess overland flow, the flood events of saturation-excess overland flow showed an increasing trend in Jingle sub-basin (Li, 2018). The current study demonstrated the results from the perspective of model parameters.

Evapotranspiration parameters

Evapotranspiration is highly affected by land cover types such as leaf area index (Zhang et al., 2014). Some researchers found that land use cover changes had greater impact on the hydrological cycle than climate change (Georgescu, 2013) and may cancel or mask the effects of climate change (Voss et al., 2002). Land use cover changes affects evapotranspiration on the regional scale mainly through vegetation changes (e.g., deforestation and afforestation, or grassland reclamation), agricultural development activities (e.g., farmland reclamation, crop cultivation, and agricultural management), and urbanization (Yang et al., 2008). Evapotranspiration change rates differ among land cover types that have different underlying surfaces (Mwangi et al., 2016). In the current study the evapotranspiration of different land use types is ranked as cultivated land > forest land > grassland > unused land, and the evapotranspiration increased year by year. Changes from forests and natural vegetation to other land use types can increase water yield and decrease evapotranspiration (Olang and Fürst, 2011). Defor-

estation and afforestation are the most influential types of land use cover changes that affect evapotranspiration (Wan et al., 2008). Olchev et al. (2008) found that transpiration and the evaporation of intercepted rainfall were reduced after tropical rainforests were converted to croplands in Indonesia. Although the land use conversion also increased soil evaporation there was overall a decrease in mean evapotranspiration. Oliveira et al. (2014) reported that deforestation reduced evapotranspiration by 36% in Brazil because the leaf area index and vegetation coverage of croplands are relatively smaller than those of forests.

Water source parameters

There are four water source parameters in the model, namely free water storage capacity (*SM*), free water storage capacity curve index (*EX*), soil effluent coefficient (*CI*) and underground diameter effluent coefficient (*CG*). *SM* is a quantitative representation of soil water storage capacity in the basin, and plays an important role in the proportion of surface runoff, interflow and underground flow. According to the previous studies (Karahan et al., 2013), *SM* has an influence on the flood peak flow, and the *SM* in the study basin showed an increasing trend. The *SM* increased and improved the free water storage reservoir in the basin. The land use change in the control basin of Jingle station increases the storage capacity of the basin. *CI* and *CG* can reflect the speed of flood submergence, and the increase of *CI* and *CG* could change the flood withdrawal curve, indicating that the soil flow and underground runoff have changed in the study area with the change of land use.

CONCLUSIONS

Based on the results from this study, the main conclusions are summarized as follows:

(1)   A new model, the modified saturation excess and infiltration excess model, had been developed based on the original saturation excess and infiltration excess model. The land uses, soil properties, rainfall and streamflow were taken as input data for the modified model. The developed *M-EIES* model is therefore used to simulate surface flow, interflow and groundwater flow. Based on the modified model, the effects of land use change on flow were investigated.

(2)   The *M-EIES* model simulated runoff within the range of acceptable accuracy, which is reflected by the goodness-of-fit measure. For model results, the efficiency of Nash and Sutcliffe for 29 flood events of the Jingle sub-basin are greater than 0.7, in both the calibration and validation periods. This indicates that the *M-EIES* model based on the original saturation excess and infiltration excess model is suitable for rainfall-runoff simulation.

(3)   Most of the model parameters showed increasing trends, but index of infiltration capacity distribution curve (*m*) showed a decreasing trend, which proved the changes of runoff generation mechanism from the perspective of model parameters in Jingle sub-basin, it can provide a new perspective for

understanding the discharge reduction in the Yellow River basin.

As a key fact causing the change in runoff, the land-use change should not be neglected, especially for its impact in the flood season. The role played by land-use change should be appropriately considered due to its impact on water resources and ecosystem health in the Fen River basin. In fact, climate change should be taken into account when assessing the impacts of land use cover change in the future. However, the compound effect of climate and land use cover change is complicated and beyond the scope of this paper. In the future research, a land use projection model based on cellular automata and Markov chain, and the regional future climate scenarios would be considered together to quantitatively predict streamflow in response to possible future land use and climate changes.

REFERENCES

Andreássian, V., Parent, E., Michel, C., 2003. A distribution-free test to detect gradual changes in watershed behavior. Water Resour. Res., 39, 9, 1252.

Apostolopoulos, T.K., Georgakakos, K.P., 1997. Parallel computation for streamflow prediction with distributed hydrologic models. Journal of Hydrology, 197, 1–24.

Blyth, K., 1993. The use of microwave remote sensing to improve spatial parameterization of hydrological models. Journal of Hydrology, 152, 103–129.

Beven, K., 1989. Changing ideas in hydrology – The case of physically-based models. Journal of Hydrology, 105, 157–172.

Beven, K., 2000a. Rainfall-Runoff Modelling: The Primer. John Wiley and Sons Ltd. Chichester, UK, 360 p.

Beven, K.J., 2000b. Uniqueness of place and process representations in hydrological modelling. Hydrol. Earth Syst. Sci., 4, 203–213.

Brown, A.E., Zhang, L., McMahon, T.A., Western, A.W., Vertessy, R.A., 2005. A review of paired catchment studies for determining changes in water yield resulting from alterations in vegetation. J. Hydrol., 310, 28–61.

Calver, A., 1988. Calibration, sensitivity and validation of a physicality based rainfall-runoff model. Journal of Hydrology, 103, 103–115.

Du, J.K., Zheng, D.P., Xu, Y.P., Hu, S.F., Xu, C.Y., 2016. Evaluating functions of reservoirs storage capacities and locations on daily peak attenuation for Ganjiang River Basin using Xinanjiang model. Chinese Geographical Science, 26, 789–802. (In Chinese with English abstract.)

Desilets, S.L.E., Nijssen, B., Ekwurzel, B., Ferré, T.P.A., 2007. Post-wildfire changes in suspended sediment rating curves: Sabino Canyon, Arizona. Hydrological Processes, 14, 1413–1423.

Duan, Q.Y., Sorooshian, S., Gupta, V.K., 1992. Effective and efficient global optimization for conceptual rainfall-runoff models. Water Resources Research, 28, 1015–1031.

Finch, J.W., Bradford, R.B., Hudson, J.A., 2004. The spatial distribution of groundwater flooding in a chalk catchment in southern England. Hydrological Processes, 18, 959–971.

Gao, G., Fu, B., Zhang, J., 2018. Multiscale temporal variability of flow-sediment relationships during the 1950s–2014 in the Loess Plateau, China. Journal of Hydrology, 563, 609–619.

Georgescu, M., 2013. Impact of anthropogenic land-use/land-cover change on climate and hydrologic cycle over the Greater Phoenix Area. Journal of Urology, 189, e872-e873.

Grayson, R.B., Moore, I.D., Mcmahon, T.A., 1992. Physically based hydrologic modeling: 2. Is the concept realistic? Water Resources Research, 28, 2659–2666.

Gonzalez-Sosa, E., Braud, I., Dehotin, J., 2010. Impact of land use on the hydraulic properties of the topsoil in a small french catchment. Hydrological Processes, 24, 2382–2399.

Jian, S., Zhao, C., Fang, S., Yu, K., 2014. Soil water content and water balance simulation of *Caragana korshinskii* Kom. in the semiarid Chinese Loess Plateau. Journal of Hydrology and Hydromechanics, 62, 89–96.

Jian, S., Wu, Z., Hu, C., Zhang, X., 2016. Sap flow in response to rainfall pulses for two shrub species in the semiarid Chinese Loess Plateau. Journal of Hydrology and Hydromechanics, 64, 121–132.

Kan, G., Li, J., Zhang, X., Ding, L., He, X., Liang, K., Jiang, X., Ren, M., Li, H., Wang, F., Zhang, Z., Hu, Y., 2017. A new hybrid data-driven model for event-based rainfall-runoff simulation. Neural Computing and Applications, 28, 2519–2534.

Karahan, H., Gurarslan, G., Zong, W.G., 2013. Parameter estimation of the nonlinear muskingum flood routing model using a hybrid harmony search algorithm. Journal of Hydraulic Engineering - ASCE, 18, 352–360.

Lee, H., Mclntyre, N., Wheater, H., 2005. Selection of conceptual models for regionalization of the rainfall-runoff relationship. Journal of Hydrology, 312, 140–147.

Liu, X., Gao, Y., Ma, S., Dong, G., 2018. Sediment reduction of warping dams and its timeliness in the Loess Plateau. Journal of Hydraulic Engineering, 49, 145–155.

Li, N., 2018. Study on the mechanism of runoff production and confluence in the Loess Plateau under the change of underlying surface. Master's Thesis. Zhengzhou University, Zhengzhou.

Luo, W.S., Hu, C.Q., Han, J.T., 1992. Research on a model of runoff yield reflecting excess infiltration and excess storage simultaneously. Chinese Journal of Water and Soil Conservation, 4, 6–13. (In Chinese with English abstract.)

Meng, C., Zhou, J., Dai, M., 2017. Variable infiltration capacity model with bgsa-based wavelet neural network. Stochastic Environmental Research and Risk Assessment, 31, 1871–1885.

Merz, B., Aerts, J., Arnbjerg-Nielsen, K., Baldi, M., Becker, A., Bichet, A., Blöschl, G., Bouwer, L.M., Brauer, A., Cioffi, F., Delgado, J.M., Gocht, M., Guzzetti, F., Harrigan, S., Hirschboeck, K., Kilsby, C., Kron, W., Kwon, H.-H., Lall, U., Merz, R., Nissen, K., Salvatti, P., Swierczynski, T., Ulbrich, U., Viglione, A., Ward, P.J., Weiler, M., Wilhelm, B., Nied, M., 2014. Floods and climate: Emerging perspectives for flood risk assessment and management. Nat. Hazards Earth Syst. Sci., 14, 1921–1942.

Molina, A., Vanacker, V., Balthazar, V., 2012. Complex land cover change, water and sediment yield in a degraded and environment. Journal of Hydrology, 472, 25–35.

Moussa, R., Voltz, M., Andrieux, P., 2002. Effects of the spatial organization of agricultural management on the hydrological behaviour of a farmed catchment during flood events. Hydrological Processes, 16, 393–412.

Mu, S., Zhou, S., Chen, Y., 2013. Assessing the impact of restoration-induced land conversion and management alternatives on net primary productivity in inner Mongolian grassland, China. Global & Planetary Change, 108, 29–41.

Mwangi, H.M., Julich, S., Patil, S.D., 2016. Relative contribution of land use change and climate variability on discharge of upper Mara River, Kenya. Journal of Hydrology Regional Studies, 5, 244–260.

Nash, J.E., Sutcliffe, J.V., 1970. River flow forecasting through the conceptual models. 1: A discussion of principles. Journal of Hydrology, 10, 282–290.

Ogden, F.L., Pradhan, N.R., Charles, W.D., 2011. Relative importance of impervious area, drainage density, width function, and subsurface storm drainage on flood runoff from an urbanized catchment. Water Resources Research, 47, 1–12.

Olang, L.O., Fürst, J., 2011. Effects of land cover change on flood peak discharges and runoff volumes: model estimates for the Nyando River basin, Kenya. Hydrological Processes, 25, 80–89.

Olchev, A., Ibrom, A., Ross, T., Falk, U., Rakkibu, G., Radler, K., Grote, S., Kreilein, H., Gravenhorst, G., 2008. A modelling approach for simulation of water and carbon dioxide exchange between multi-species tropical rain forest and the atmosphere. Ecological Modelling, 212, 122–130.

Oliveira, P.T.S, Nearing, M.A., Moran, M.S., 2014. Trends in water balance components across the Brazilian Cerrado. Water Resources Research, 50, 7100–7114.

Park, D., Markus, M., 2014. Analysis of a changing hydrologic flood regime using the variable infiltration capacity model. Journal of Hydrology, 515, 267–280.

Pathiraja, S., Marshall, L., Sharma, A., 2016. Hydrologic modeling in dynamic catchments: A data assimilation approach. Water Resources Research, 52, 3350–3372.

Pirastru, M., Castellini, M., Giadrossich, F., Niedda, M., 2013. Comparing the hydraulic properties of forested and grassed soils on an experimental hillslope in a Mediterranean environment. Procedia Environmental Sciences, 19, 341–350.

Ren, L, Shen, H., Yuan, F., Zhao, C., Yang, X., Zheng, P., 2016. Hydrological drought characteristics in the Weihe catchment in a changing environment. Advances in Water Science, 27, 492–500. (In Chinese with English abstract.)

Rogger, M., Agnoletti, M., Alaoui, A., Bathurst, J.C., Bodner, G., Borga, M., Chaplot, V., Gallart, F., Glatzel, G., Holko, L., Horn, R., Kiss, A., Kohnová, S., Leitinger, G., Lennartz, B., Parajka, J., Perdigão, R., Peth, S., Plavcová, L., Quinton, J.N., Salinas, J.L., Santoro, A., Szolgay, J., Tron, S., van den Akker, J.J.H., Viglione, A., Blöschl, G., 2017. Land use change impacts on floods at the catchment scale: Challenges and opportunities for future research. Water Resour. Res., 53, 7, 5209–5219. DOI: 10.1002/2017WR020723.

Rozalis, S., Morin, E., Yair, Y., Price, C., 2010. Flash flood prediction using an uncelebrated hydrological model and radar rainfall data in a Mediterranean watershed under changing hydrological conditions. Journal of Hydrology, 394, 245–255.

Sorooshian, S., Duan, Q., Gupta, V.K., 1993. Sthocastic parameter estimation procedures for hydrologic rainfall-runoff models: Correlated and heteroscedastic error cases. Water Resource, 29, 1185–1194.

Uchida, E., Xu, J.T., Rozelle, S., 2005. Grain for green: Cost-effectiveness and sustainability of China's Conservation Set-Aside Program. Land Economics, 81, 247–264.

Viglione, A., Merz, B., Dung, N.V., Parajka, J., Nester, T., Blöschl, G., 2016. Attribution of regional flood changes based on scaling fingerprints. Water Resour. Res., 52, 5322–5340.

Voss, R., May, W., Roeckner, E., 2002. Enhanced resolution modelling study on anthropogenic climate change: changes in extremes of the hydrological cycle. International Journal of Climatology, 22, 755–777.

Wagener, T., McIntyre, N., Lees, M.J., Wheater, H.S., Gupta, H.V., 2003. Towards reduced uncertainty in conceptual rainfall-runoff modeling: Dynamic identifiability analysis. Hydrol. Processes, 17, 455–476.

Wagener, T., 2007. Can we model the hydrological impacts of environmental change? Hydrol. Processes, 21, 3233– 3236.

Wagener, T., Sivapalan, M., Troch, P.A., McGlynn, B.L., Harman, C.J., Gupta, H.V., Kumar, P., Rao, P.S.C., Basu, N.B., Wilson, J.S., 2010. The future of hydrology: An evolving science for a changing world. Water Resour. Res., 46, W05301.

Wallner, M., Haberlandt, U., 2015. Non-stationary hydrological model parameters: a framework based on SOM-B. Hydrological Processes, 29, 3145–3161.

Wan, R., Shan, G., 2004. Progress in the hydrological impact and flood response of watershed land use and land cover change. Journal of Lake Science, 16, 3, 258–264.

Wang, T., Istanbulluoglu, E., Wedin, D., Hanson, P., 2015. Impacts of devegetation on the temporal evolution of soil saturated hydraulic conductivity in a vegetated sand dune area. Environmental Earth Sciences, 73, 1–10.

Yang, X., Ren, L., Yong, B., Wei, Z., 2008. The impact of land use change on hydrological cycle at a semiarid headwater catchment in north china. In: Education Technology & Training & International Workshop on Geoscience & Remote, 2, pp. 508–512.

Yüksek, T., Göl, C., Yüksek, F., Yüksel, E.E., 2009. The effects of land-use changes on soil properties: the conversion of alder coppice to tea plantations in the humid northern Black Sea region. African Journal of Agricultural Research, 4, 665–674.

Zhang, Y., Guan, D., Jin, C., Wang, A., Wu, J., Yuan, F., 2014. Impacts of climate change and land use change on runoff of forest catchment in northeast China. Hydrological Processes, 28, 186–196.

Zhao, R.J., 1992. The Xinanjiang model applied in China. Journal of Hydrology, 135, 371–381. (In Chinese with English abstract.)